Classification: Biological Sciences (Medical Sciences) / Physical Sciences (Chemistry)

Title: Metabolic profiles as putative predictors of relapse in pediatric brain tumour using direct surface and imaging mass spectrometry

Authors: Joris Meurs[a], David J. Scurr[a], Lisa C.D. Storer[b], Richard G. Grundy[b], Morgan R. Alexander[a], Ruman Rahman[b] & Dong-Hyun Kim[a,1,*]

[a]: Advanced Materials & Healthcare Technologies Division, School of Pharmacy, University of Nottingham, UK

[b]: Children's Brain Tumour Research Centre, Biodiscovery Institute, School of Medicine, University of Nottingham, UK

[1]: To whom corresponding may be addressed. E-mail: dong-hyun.kim@nottingham.ac.uk

Keywords: pediatric ependymoma, metabolite profiling, LESA-MS/MS, 3D OrbiSIMS, tumor biology, tissue microarray

Abstract

Surgically-resected biopsies from childhood brain tumors are archived in a formalin-fixed paraffin-embedded (FFPE) state. Identified key tumor regions are conserved through the fabrication of tissue microarrays (TMA). The vast amount of TMA libraries available have the potential to be used for metabolite profiling; however, due to incompatibility of TMAs with current analysis strategies, the potential has been unexplored. The recent emergence of liquid extraction surface analysis tandem mass spectrometry (LESA-MS/MS) and Orbitrap secondary ion mass spectrometry (3D OrbiSIMS) allows for a novel untargeted metabolite profiling and imaging approach for characterization of tumor TMAs. This strategy employs serial mass spectrometry (MS) analysis, with the high mass resolving imaging power of 3D OrbiSIMS combining complementarity, with the detection of a greater number of metabolites using LESA-MS/MS. Using multivariate analysis on data generated from both techniques permits the identification of metabolites that group patients based on eventual tumor recurrence, leading to the discovery of novel affected metabolic pathways and the prediction of tumor recurrence with high confidence. Moreover, both techniques reveal a unique set of classifiers and metabolic pathways for predicting pediatric ependymoma relapse from a set of primary tumors. The serial MS strategy opens new opportunities to retrospectively link molecular data from any FFPE TMA library with clinical outcomes and to discover novel drug targets with the aim of developing stratified drug treatments.

Statement of significance

Valuable and rare tumor tissue, such as from pediatric brain, is typically conserved through the creation of tissue microarrays (TMA) as the same biopsy tissue can be cored repeatedly. The small amount of sample has been a considerable obstacle for many modes of metabolomic analyses, which routinely require larger amounts of tissue. Using serial direct mass spectrometry techniques and multivariate analysis, tumor recurrence was predicted from differences in ion intensity, and novel and unique metabolic pathways in tumor relapse were discovered. This ability to retrospectively acquire metabolomic information from TMA archives will have a huge impact on understanding tumor

development, heterogeneity and relapse to facilitate the development of personalized therapies that target pediatric brain tumor metabolism.

Introduction

Central nervous system (CNS) pediatric tumors are the most prevalent type of solid cancer diagnosed in children (1) and the leading cause of mortality among all cancers in children (1). From the clinical and biological perspective, intracranial pediatric ependymomas (pEPNs) remain enigmatic and challenging tumors to treat. Overall, the prognosis is poor with over 50% of tumors relapsing and less than 50% of children surviving this disease (5-year overall survival is ~25% for patients who have relapsed (2–4)). Though widely considered a 'surgical disease', a significant proportion of patients relapse, even following complete surgical resection of the tumor. The identification of biological correlates of disease progression and patient-tailored therapeutic targets therefore remains a significant challenge in this disease. Understanding the biochemical nature of tumor development is of vital importance for the development of the next-generation of treatments (2). In a disease state, the human metabolome is affected by several factors and therefore provides an excellent source of information to investigate disease-related alterations in metabolism (5). To do so, an untargeted metabolomics approach can be used to study molecular changes within and between tissue samples of different phenotypes (6, 7). State-of-the-art metabolomics techniques allow the detection of hundreds to thousands of metabolites in a sample (8), where untargeted metabolomics of cancer tissue is undertaken using liquid chromatography-mass spectrometry (LC-MS) and gas chromatography-mass spectrometry (GC-MS) (9, 10). Chromatography-based strategies allow the identification of a vast number of metabolites; however these require 20-50 mg of tissue for metabolomics analysis.

Preserving tumor regions of interest is commonly done using the tissue microarray (TMA) format. The neuropathologist identifies and cuts out key regions in the whole tissue section which are stored as a separate FFPE block. The TMA platform allows small amounts of tissue to be used for transcriptomic

and histological analysis (11–13), though for diagnosis the entirety of the tumor needs to be reviewed. Since the TMA tissue sections are small (diameter <1 mm; thickness: 4 µm), sensitive analytical techniques are required for metabolomic studies in order to detect low-abundance metabolites. Despite the vast amount of available TMA libraries, metabolite profiling of tumor TMAs has been an unexplored territory due to incompatibility of LC-MS or GC-MS analysis. In order to perform MS analysis on TMA, a technique is required to directly obtain a wide range of metabolites from tissue sections.

A few studies have shown the potential of liquid extraction surface analysis-mass spectrometry (LESA-MS) for untargeted metabolomics across a range of sample types. With LESA-MS, liquid microjunction-based extraction can be performed on a flat sample surface to obtain the analytes of interest which are directly injected into the mass spectrometer (14). Hall *et al.* (15) found significantly changed profiles of lipids in non-alcoholic fatty liver disease (NAFLD) tissue using LESA-MS. This allowed discrimination between different stages of stearosis. Ellis *et al.* (16) used LESA-MS for the analysis of single-cell arrays and could distinguish cell types based on lipid profiles showing the capability of performing single cell metabolomics with LESA. We have also (17) successfully used LESA-MS to identify metabolic changes on small volumes of urine samples from an intervention study. Basu *et al.* (18) used LESA-MS for direct metabolite profiling for several different breast cancer cell lines. The capability of LESA was shown to allow direct analysis of adherent cells with minimal sample preparation. Collectively, these studies have shown that from a limited amount of sample, metabolic changes could be measured.

The recent development of 3D OrbiSIMS, revealed new possibilities for metabolic profiling due to its capability of high mass accuracy and mass resolving power (>240,000 at m/z 200) at subcellular spatial resolution(19). In that study, it was shown that 3D OrbiSIMS can be used for 2D and 3D imaging of neurotransmitters, in situ identification of lipid species using tandem MS, and performing metabolomics profiling of single cells (19). One unmet scientific challenge for brain tumor research is

to perform metabolomics analysis to understand tumor development and find potential targets for therapies (8, 20). Previous research by Gularyan *et al.* (21) has shown the capability of time-of-flight secondary ion mass spectrometry (ToF-SIMS) for analysis of formalin-fixed paraffin-embedded (FFPE) glioblastoma tissue, to study inter- and intra-tumor heterogeneity. Further, direct MS metabolite profiling using desorption electrospray ionization-mass spectrometry (DESI-MS) has been successfully used to discriminate between glioma and meningioma, and distinguish healthy tissue regions from cancerous tissue (22–24). However, in the ToF-SIMS and DESI-MS studies whole FFPE and fresh frozen tissue sections were used.

It has been reported that mass spectrometry is not the preferred method of choice for *ex vivo* metabolomics on brain tumors due to the requirement to extract the metabolites for analysis which prevents subsequent analysis of the valuable sample (1). 3D OrbiSIMS and LESA tandem mass spectrometry (LESA-MS/MS) require only minimal sample preparation, analysis can be performed directly on the tissue sample, and both instruments can acquire data in an automated manner using the TMA sample platform. These MS techniques can therefore circumvent the need for tissue homogenization, allowing the tissue to remain architecturally intact and available for subsequent study. The data achievable using this approach will address current challenges in cancer metabolomics, as detection of low abundance (highly polar) oncometabolites to study important metabolic pathways, may enable the development of novel diagnostic and treatment strategies (9, 25). To date and to the best of our knowledge, no studies have thus far reported the use of combined 3D OrbiSIMS and LESA-MS/MS for untargeted metabolite profiling on TMAs. Combining MS techniques, in which ions are generated via different mechanisms, will allow acquisition of complementary metabolomic datasets from the same set of samples. Combination of the individual datasets on existing TMA archives could therefore provide a vast amount of clinically valuable information. Here, we perform 3D OrbiSIMS and LESA-MS/MS analysis of FFPE pediatric ependymoma TMAs as an exemplar demonstration of the ability to perform untargeted surface metabolomics and obtain clinically relevant data.

Results & Discussion

Serial 3D OrbiSIMS and LESA-MS/MS for *in situ* metabolite profiling. We analyzed de-paraffinized TMAs (**Fig. 1***A-B* and S1), first with 3D OrbiSIMS (**Fig. 1***C*), followed by LESA-MS/MS (**Fig. 1***D*). The 3D OrbiSIMS was introduced to enable the imaging of metabolites within the individual TMA sections and to obtain the *in situ* spatial metabolite profile of FFPE ependymoma tissue. During SIMS analysis, the sample is slightly etched by the primary ion beam (20 kV Ar_{3000}^{+}), although the amount of sample consumed by SIMS is limited when argon clusters are used (28). Prior analysis by 3D OrbiSIMS did not lead to a decrease in either the number of detected ions (Student's *t*-test: p = 0.2578) or ion intensity (Student's *t*-test: p = 0.1806) for LESA-MS/MS data (**Fig. S2**), indicating that subsequent metabolite profiling with LESA-MS/MS can be performed without data loss. LESA (**Fig. 1***D*) is a micro junction-based extraction technique that allows fully automated extraction and direct MS analysis (14). Tandem MS was used here to allow for more confident identification of metabolites. After the spectral data acquisition, data were processed in MATLAB for using a multivariate analysis algorithm (**Fig. 1***E-H*)

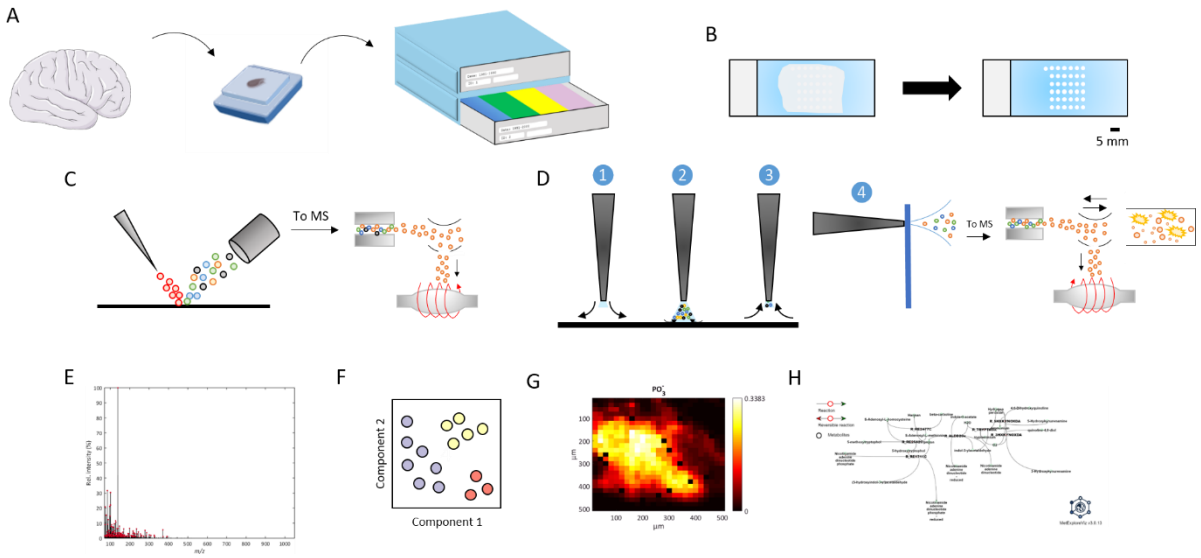

Fig. 1: Serial mass spectrometry analysis of pediatric ependymoma tissue microarrays. (A) After surgical resection, the tumor area was marked and then paraffin-embedded for long term storage. (B) For MS analysis, a TMA block from the archive was sectioned and mounted onto a glass substrate followed by a xylene wash to remove the paraffin. (C) Paraffin-free samples were then analyzed by 3D OrbiSIMS followed by (D) LESA-MS/MS. (E) Ions were selected from the mass spectra and aligned. (F)

Subsequently, data were subjected to partial-least squares-discriminant analysis (PLS-DA) to identify discriminative ions for tumor recurrence. (G) Those ions were then used to explore the heterogeneity of selected metabolites between tumors using MS imaging and (H) to identify affected pathways.

Complementary metabolite profiling with 3D OrbiSIMS and LESA-MS/MS. The use of direct MS has not been reported yet for ependymoma metabolite profiling due to the small quantity of tissue available per patient. Tumor sections on a TMA range in diameter from 0.6 to 1.0 mm and are approximately 4 µm thick. 3D OrbiSIMS and LESA-MS/MS are both applicable to sub-millimeter sample size and therefore present an opportunity to obtain novel MS data from extremely small tissue quantities. Furthermore, the relatively non-destructive nature of the 3D OrbiSIMS allows for subsequent analysis of the same sample by multiple techniques. MS^1 spectra acquired from the TMAs with 3D OrbiSIMS and LESA were processed to obtain ion intensities. A higher number of putative identifications (**Fig. 2***A*) were observed in the LESA (annotated ions: 634 (+), 51 (-)) compared to 3D OrbiSIMS data (annotated ions: 86 (+), 116 (-)). Annotated metabolites in 3D OrbiSIMS spectra were found to be mostly (hetero)aromatic compounds whilst with LESA, linear polar and non-polar molecules were detected (**Fig. 2***B*). Comparison of annotated metabolite classes revealed that 60 classes were commonly detected with 3D OrbiSIMS and LESA-MS whilst 20 and 83 classes were uniquely detected by 3D OrbiSIMS and LESA-MS, respectively (**Fig. 2***C*). To confirm metabolite identities, LESA-MS/MS spectra were compared against a library (mzCloud). In total, 288 metabolites were identified within 4 minutes of LESA-MS/MS analysis time per sample. The number of identified metabolites is a vast improvement compared to previous research conducted on metabolite profiling of ependymoma tissue using NMR where respectively, 18 and 25 metabolites were identified and quantified (1, 26).

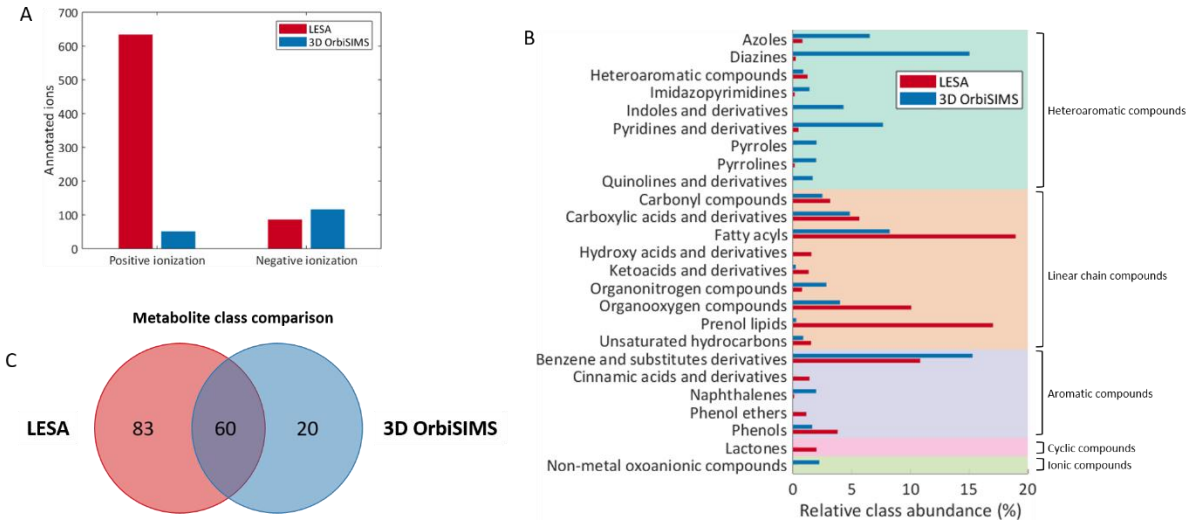

Fig. 2: Identifying putative metabolites in 3D OrbiSIMS and LESA-MS spectra. (A) In total, more ions were identified in the LESA-MS spectra, though the number of ions in negative mode identified as metabolite was higher for SIMS. (B) For all identified ions, the class as described in the Human Metabolome Database was obtained to identify which classes can be detected with each technique. The patched areas represent structurally similar classes. (C) A Venn diagram was derived with data from both surface MS techniques, identifying common and unique metabolite classes that could therefore provide complementary and additive information.

Previous NMR research showed that pediatric ependymoma had higher levels of *myo*-inositol and glutathione compared to other cerebellar tumors (1). Furthermore, levels of *myo*-inositol, glucose, and alanine could be used to classify pediatric ependymoma tissue, relative to non-ependymoma tissue (1). Here, the sample pool consisted of ependymoma tissue only. From the LESA-MS/MS identified components, lactate, leucine/isoleucine, succinate and valine were common to previously identified ubiquitous metabolites in ependymoma (1, 26) and were found across all ependymoma samples. Cuellar-Baena *et al.* (26) noted high levels of *myo*-inositol in the NMR spectra to be characteristic of pediatric ependymoma. In the LESA-MS spectra (**Fig. S3***A*), the ion (*myo*-inositol identified putatively) at *m/z* 203.0526 ($[M+Na]^+$) is on average only about 0.2% of the base peak intensity. A reason for this relatively low ion intensity can be attributed to an ion suppression effect due to the lack of separation (chromatography) prior to ionization (29). In addition, the ion intensity cannot solely be attributed to *myo*-inositol due to the potential presence of isobaric compounds such as glucose and other potential isomers. Using direct MS, *myo*-inositol could be resolved from glucose

and other isobaric hexosaccharides at MS^2 level, though it cannot be distinguished from its epimers (30). Despite the relatively low intensity of the ion at *m/z* 203.526, the *myo*-inositol intensity was found to be stable across all seven patients analyzed (ANOVA: p = 0.4778; **Fig S3***B*). This supports the findings of Bennet *et al.* (1) that *myo*-inositol is a suitable metabolite to discriminate pediatric ependymoma from other CNS tumors.

Furthermore, 10 highly abundant MS/MS identified metabolites were observed that have not been reported for ependymoma (1, 26). Those observed metabolites were 16-hydroxyhexadecanoic acid, *trans*-3-hexenoic acid, 4-hydroxybenzaldehyde, 3,4-dimethylbenzoic acid, carvone, methyl palmitate, decanoic acid, diethanolamine, and 3-hydroxymethylglutaric acid. These compounds were submitted to MetExplore (31, 32) for metabolic network analysis. Decanoic acid was found to be part of a known metabolic pathway (fatty acid biosynthesis). The exact relevance of this pathway to pediatric ependymoma is currently unknown; however, fatty acid metabolism has been reported as an affected pathway in other types of cancer (33, 34).

Improvements can still be made on the annotation of metabolites in SIMS spectra. In both LESA and 3D OrbiSIMS, ions are generated in a complementary manner. Whilst nanoESI predominantly generates adduct ions of the parent molecule, SIMS spectra can contain numerous peaks which can be either intact molecules or fragments thereof (35). This makes the automated assignment of SIMS secondary ions to metabolite identities a challenge. Using the Human Metabolome Database, only 4% of the 3D OrbiSIMS ions could be annotated compared to 28% for ions in the LESA-MS spectra.

Predicting tumor recurrence from metabolite profiles. Ependymoma TMA samples were analyzed with 3D OrbiSIMS followed by LESA-MS/MS and processed using a custom MATLAB script for peak picking, alignment and multivariate analysis. To investigate the potential of the serial MS strategy for oncometabolomics, samples were categorized by eventual tumor recurrence. Analyzed tumor sections consisted of 7 primary tumors with each three replicates, though for 5 out of 7 patients in this dataset, the tumor recurred at least once after surgery or follow-up treatment (**Tab. 1**). From a

diagnostic and therapeutic point of view, it is of interest to predict if patients will experience tumor relapse or if primary treatment is successful so therapy can be adjusted consequently.

To compare the utility of the assignments from the two techniques, they have here been treated separately. Ion intensity matrices for LESA-MS data were normalized to the total ion count (TIC) and log-transformed. Processed data matrices were individually subjected to partial-least squares-discriminant analysis (PLS-DA) to identify mass ions for predicting tumor recurrence. The patient data separated into two distinct groups with recurring samples scoring more highly in both the first and second component (**Fig. 3***A*). The model was validated using leave-one-out cross-validation, showing accurate predictivity for tumor recurrence using the LESA-MS data acquired in positive mode (R^2: 0.9845; Q^2: 0.4751). A Q^2 value greater than 0.4 is acceptable for biological models (36). As determined by permutation testing (37), the PLS-DA model performed significantly better than a PLS-DA model with randomly assigned group labels ($p = 0.0345$). LESA-MS data acquired in negative mode did not display good predictivity of tumor recurrence (Q^2: 0.0154). Ion intensities from the LESA-MS data acquired in positive mode with a variable importance in projection (VIP) score higher than 1.5 were considered discriminative (**Fig. 3***B*). Those ions (total: 31) were subjected to Student's t-test followed by a permutation test to estimate the false discovery rate (FDR). Significant ions ($p < 0.05$; **Fig. 3***C*) were annotated using the Human Metabolome Database (38) (5 ppm mass tolerance; charge state: 1+).

The annotated ions were thereafter submitted for pathway analysis in MetExplore (31, 32). Linoleate metabolism and fatty acid oxidation were putatively identified as affected pathways. In the fatty acid oxidation pathway, metabolic reactions involving 4,8 dimethylnonaoyl carnitine were upregulated (**Fig. 3***D1*). The affected pathways in lineoleate metabolism was more prominent in the relapse group for the conversion of epoxy fatty acids (EpOMEs) to fatty acids and vice versa (**Fig. 3***D*2-3). Although the role of these pathways in ependymoma is presently unknown, fatty acid metabolism plays an important role in carcinogenesis (39). Furthermore, fatty acid oxidation has been reported before to

be an important pathway in cancer metabolism (40). The relative increase in abundance of putatively identified 9(10)-EpoME/12(13)-EpoME and 4,8 dimethylnonaoyl carnitine could provide the clinician with valuable information towards predicting tumor recurrence. For both putatively assigned ions, receiver operating characteristic (ROC) curves were created and area under the curve (AUC) of 0.8333 and 0.9000 were found respectively (**Fig. 3***E*), indicating that both putatively identified ions serve as accurate classifiers for tumor relapse. The identified classifiers provide then a tool for clinicians to predict relapse for surgically-resected primary ependymoma. Therefore, the LESA-MS data presented shows great potential for the use of direct MS-based metabolomics of cancer tissue TMAs by unravelling currently unknown affected metabolic pathways and identification of classifiers to predict tumor recurrence.

Table 1: Demographic information for patients included in the analysis (*N* = 7; *n* = 3)

Age at diagnosis	55.3 ± 39.9 months
Gender	Female (N = 5); Male (N = 2)
Recurrence	Yes (N = 5); No (N = 2)
WHO grade	II (N = 4); III (N = 3)
Overall survival	60.1 ± 35.1 months
Status	Alive (N = 4); Death (N = 3)

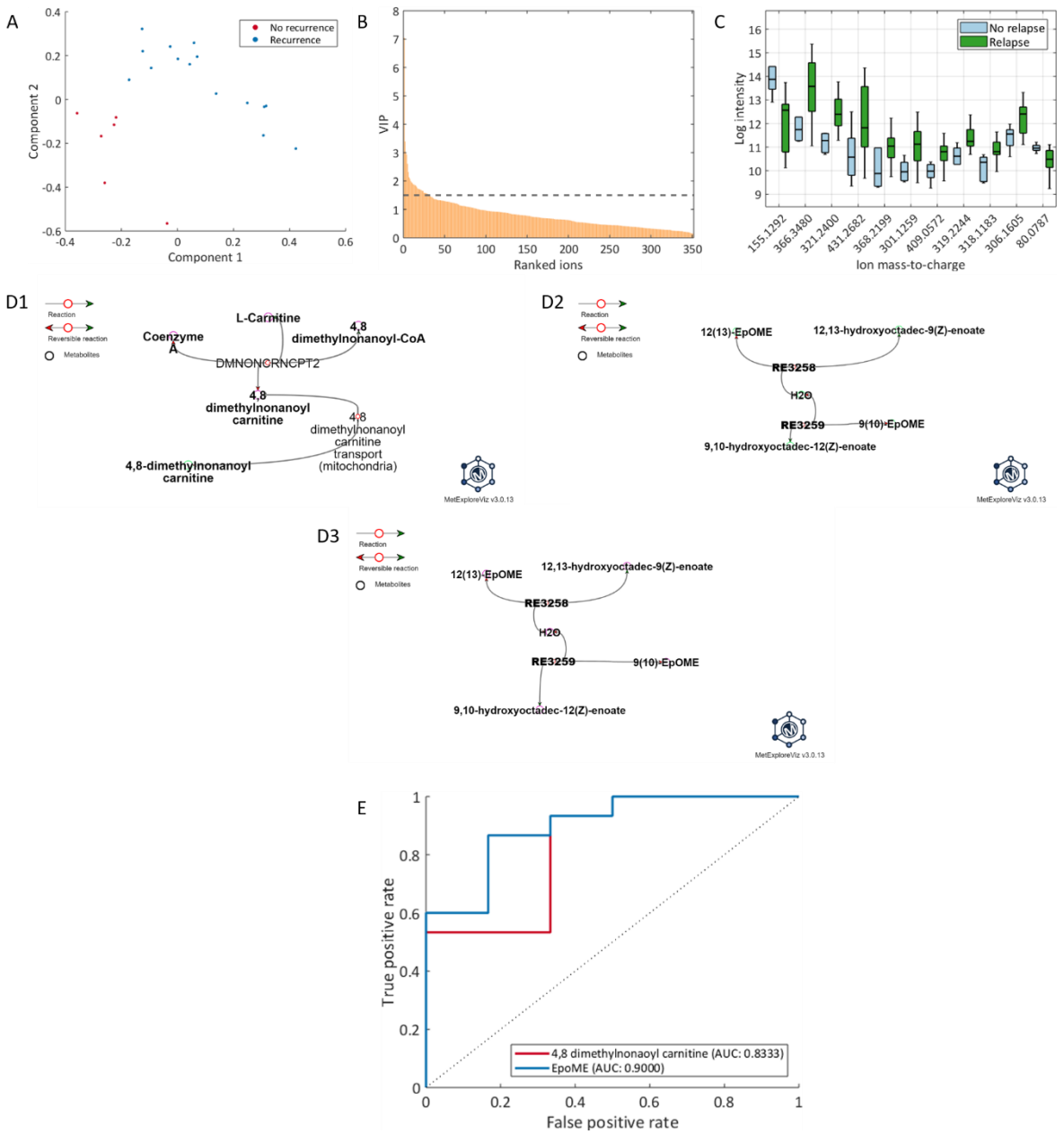

Fig. 3: Prediciting tumor recurrence from LESA-MS data using PLS-DA. (A) The PLS scores plot for the first and second component show clustering of patients for which the tumor recurred (B) Ranked plot of VIP scores of the PLS-DA model (R^2: 0.9845; Q^2: 0.4751) followed by (C) univariate statistical analysis, were performed to identify significantly altered metabolites. (D) Significant annotated metabolites were subjected to pathway analysis and revealed two affected pathways, (D1) fatty acid oxidation and (D2-3) linoleate metabolism, associated with ependymoma recurrence. (E) ROC curves for putatively identified metabolites in affected pathways.

The 3D OrbiSIMS data were treated in the same manner as the LESA-MS, i.e. ion intensities were TIC normalized, log-transformed and subjected to PLS-DA. 3D OrbiSIMS data acquired in positive mode did not have any value for predicting tumor recurrence (Q^2: -0.0338). Data acquired in negative mode

showed some degree of patient grouping based on relapse and bore some predictive value (R^2: 0.8119; Q^2: 0.3095; **Fig. 4***A*). In total, 14 ions were found to be discriminative (VIP > 1.5; **Fig. 4***B*), from which 10 showed a statistically significant difference in abundance between *no relapse* and *eventual relapse* primary tumors (**Fig. 4***C*). Significant ions were annotated using the HMDB and annotations were thereafter submitted to MetExplore to identify affected pathways. We found that three pathways were potentially affected by a change in metabolite abundance. Those pathways (tryptophan metabolism, tyrosine metabolism, and phenylalanine metabolism) were less prominent in the tumor relapse group (**Fig. 4***D*). The importance of amino acid metabolism has been recognized for targeting cancer treatment development (41, 42). Previous work on metabolite profiling showed higher levels of L-phenylalanine in pediatric ependymoma compared to other pediatric brain tumors (26). Here, it was observed that L-phenylalanine levels were higher in the *no relapse* primary tumor group compared to the *eventual relapse* primary tumor group, indicating that relatively lower levels of L-phenylalanine could play an important role in tumor relapse. Because each technique detected different ions and consequently metabolites, the 3D OrbiSIMS identified metabolic pathways which we could not identify by LESA-MS. This shows that the use of complementary direct MS techniques to perform serial analysis on TMAs reveals useful, additive and clinically relevant information. In the same manner as for the LESA-MS data, ROC curves were generated for putatively annotated metabolites from the 3D OrbiSIMS spectra (**Fig. 4***E*). L-phenylalanine, 4,6-hydroxyquinoline and 5-hydroxytryptophol were found to be perfect classifiers for tumor recurrence. Adrenochrome and β-carboline had AUC values of 0.9889 and 0.9778 respectively, indicating that these metabolites are also excellent classifiers for tumor recurrence. This provides the clinician with a complementary set of metabolic classifiers for predicting relapse from resected primary ependymoma.

Although only a small number of patients were used in this study, the data support the potential for performing large-scale studies on TMA libraries to investigate the *in situ* alterations of metabolite profiles and affected pathways between tumor phenotypes using LESA-MS and 3D OrbiSIMS. Rather than finding the same classifiers, performing analysis with both direct MS techniques allowed us to

discover unique classifiers and metabolic pathways for predicting ependymoma relapse from metabolic signatures in primary ependymoma. This provides an opportunity to perform a clinical study on available libraries of FFPE tumor TMAs. Furthermore, novel pathways have been discovered that provide insight into potential tumor relapse which will improve upon understanding of tumor biology (26) and eventually leading to the discovery of new drug targets, which may prevent or delay tumor relapse.

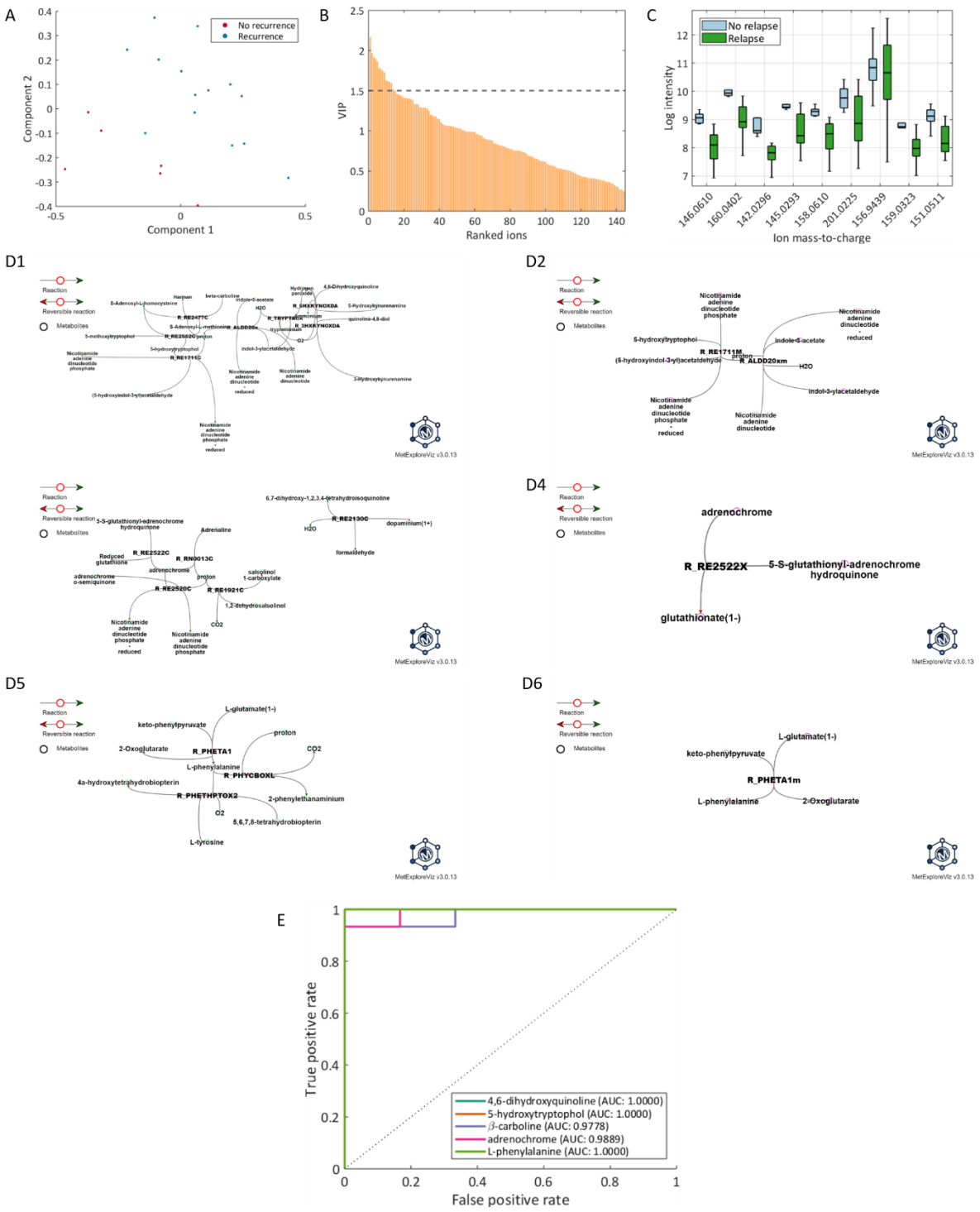

Fig. 4: Predicting tumor recurrence from 3D OrbiSIMS data using PLS-DA. (A) The PLS scores plot for the first and second component show clustering of patients for which the tumor recurred. (B) Ranked VIP scores for LESA-MS ions (C) followed by univariate statistical analysis were performed to identify significantly altered metabolites. Pathway analysis in MetExplore revealed significant affected pathways for tryptophan metabolism in (D1) the cytoplasm and (D2) mitochondria, tyrosine metabolism in the (D3) cytoplasm and (D4) peroxisome, and phenylalanine metabolism in the (D5) cytoplasm and (D6) mitochondria, all of which were putatively associated with ependymoma recurrence. (E) ROC curves for putatively identified metabolites in affected pathways.

Investigation of metabolite heterogeneity between tumor sub-groups. It is well known that pediatric ependymoma is characterized by a high degree of inter-patient genetic, epigenetic and metabolic heterogeneity, which manifests as distinct tumor sub-groups with varying prognoses (26, 43). However, it is not yet known whether metabolomic profiles vary within intra-tumor regions of pediatric ependymoma and/or within distinct ecological niches.

The capability of SIMS for studying intra- and inter-tumor heterogeneity has been shown by Gularyan *et al.* (21). Here, we performed MS imaging (MSI) with 3D OrbiSIMS. Using 3D OrbiSIMS, only a small area of tissue (~ 1 mm diameter) is required to study intra- and inter-tumor heterogeneity, allowing a better understanding of tumor development on a microscale level. Through untargeted metabolomics, we putatively identified phenylalanine metabolism as a prominent pathway. Here, the distribution of L-phenylalanine (*m/z* 146.0610 $[M-H-H_2O]^-$) across intra-tumor regions was investigated using the 3D OrbiSIMS chemical images. Understanding the phenomena of heterogeneity is an important step towards developing personalized therapies (44). MSI was performed on a 500 µm × 500 µm area. The total ion images for the 3D OrbiSIMS data are added as supplement (**Fig. S4-5**). In the *eventual relapse* group (**Fig. 5***A*), the presence of L-phenylalanine appears to be lower across the analyzed area compared to the *no relapse* group (**Fig. 5*B***) based on the observation of a significantly lower ion frequency across the image (Mann-Whitney test: $p = 5.29 \times 10^{-4}$; **Fig. 5**C). It was already observed that the total L-phenylalanine intensity was significantly lower (Student's *t*-test: $p = 4.31 \times 10^{-4}$) in the *eventual relapse* compared to *no relapse* group from the OrbiSIMS data acquired in negative mode (**Fig. 4***C*). In concordance with the reduced ion intensity for L-phenylalanine in the summed 3D OrbiSIMS spectra, it was found that the average pixel L-phenylalanine secondary ion intensity was significantly lower (Student's *t*-test: $p = 2.12 \times 10^{-5}$) for the *eventual relapse* group (**Fig. 5***D*). The heterogeneity across the sample was investigated for L-phenylalanine across the analyzed area. The ion images reveal a heterogeneous distribution of L-phenylalanine secondary ion intensity across the analyzed tissue area. Here, we used the dynamic range (the ratio of the maximum and minimum ion intensity) to compare the range of amounts observed across the image and therefore to

estimate the heterogeneity between tumor groups (primary and relapse) (45). To investigate the degree of heterogeneity, L-phenylalanine was compared to the spatial distribution of adenine (*m/z* 134.0467 $[M-H]^-$; **Fig. 5***E*). For adenine, we observed a lower intensity pixel-to-pixel intensity range, interpreted as a more homogeneous distribution across the tumor area in both groups (ANOVA: p = 0.0039). Increased intra-tumor heterogeneity has previously been identified as an important indicator for therapy resistance and poor overall survival (46–48). However, for L-phenylalanine, we did not observe a difference in heterogeneity (dynamic range) between both groups (Student's *t*-test: p = 0.9443; **Fig. 5***F*). This could be a potential indicator that intra-tumor heterogeneity in primary ependymoma does not have a predictive value for eventual relapse.

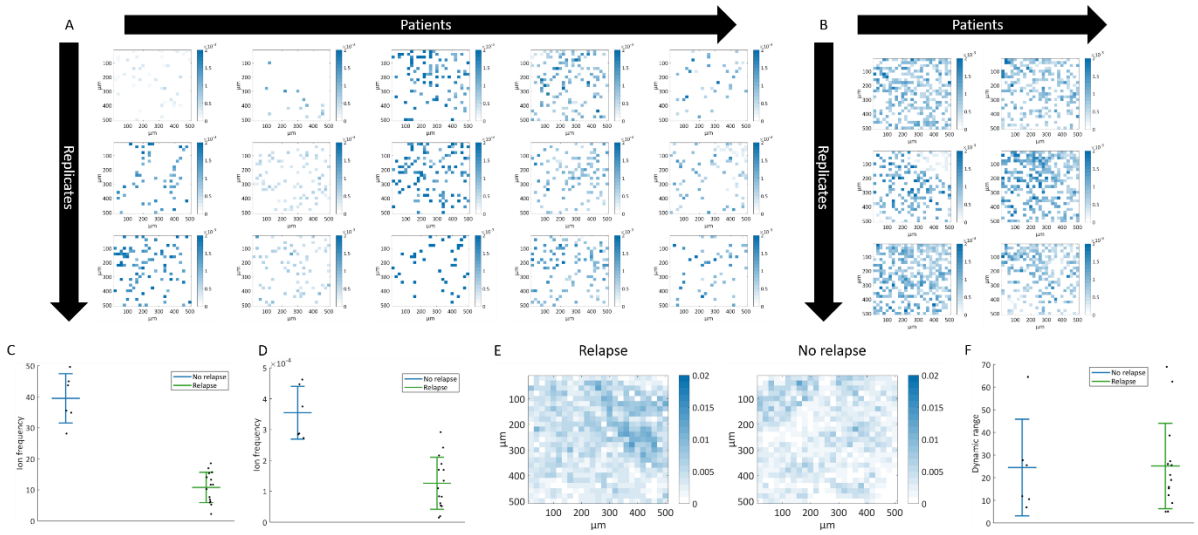

Fig. 5: Comparison of L-phenylalanine (*m/z* 146.0610 $[M-H-H_2O]^-$) distribution in OrbiSIMS images for pediatric ependymoma. Ion images for L-phenylalanine in (A) the *no relapse* group and (B) the *eventual relapse* group. (C) The occurrence (spatial frequency) throughout the image of L-phenylalanine was found to be higher in the non-relapse group. (D) It was also observed that the average intensity per pixel of L-phenylalanine was higher in the non-relapse group. (E) Representative 3D OrbiSIMS images for adenine. The dynamic range for adenine was significantly smaller compared to L-phenylalanine (ANOVA: p = 0.0039). (F) No difference in heterogeneity was observed for L-phenylalanine between the *no relapse* group and *eventual relapse* group.

The demonstrated methodology will be able address currently neglected or underexplored oncometabolomic research questions, which could be broadly extended to other fields restricted by sample scarcity. This strategy when combined with multivariate analysis, allowed us to identify

discriminative metabolites, to accurately predict tumor recurrence and to discover novel affected pathways for tumor recurrence on a relatively small number of patients.

Conclusions

In this study we have demonstrated that *in situ* metabolite profiles of pediatric ependymoma TMAs can be obtained with serial MS analysis using 3D OrbiSIMS and LESA-MS/MS, conducted using the same tissue section. The amount of sample required for analysis is small (~1 mm diameter and 4 µm thick) and therefore the serial MS workflow is a competitive alternative to standard metabolomics analysis using LC-MS, GC-MS, or NMR. With LESA-MS, we putatively identified 12(13) EpoME/9(10) EpoME and 4,8 dimethylnonaoyl carnitine as accurate predictors of tumor recurrence. Using 3D OrbiSIMS, we found a set of complementary putatively identified metabolites, from L-phenylalanine, 4,6-hydroxyquinoline and 5-hydroxytryptophol, which were found to be classifiers to distinguish between no relapse and eventual relapse. The use of serial analysis here was essential since using both techniques revealed novel complementary pathways that would not have been identified using only either of the techniques alone. Another indicator for tumor relapse was identified using the imaging capability of 3D OrbiSIMS. L-phenylalanine had a significantly reduced intensity per pixel and the frequency of detection was significantly lower between the *eventual relapse* (N = 5; n = *3*) and *no relapse* group (N = 2; n = 3). Furthermore, the identification of highly abundant metabolites (and associated pathways) with LESA-MS/MS, ubiquitous to distinct intra-tumor regions within a TMA core, may indicate critical metabolic processes, offering potential therapy avenues which circumvent genetic heterogeneity. Such highly abundant metabolites could potentially be used for improved diagnosis and MSI could aid in spatial metabolomics of histologically different microenvironments.

Materials and Methods

Tissue microarray preparation. Hematoxylin and eosin-stained sections from FFPE pediatric ependymoma were examined by a neuropathologist at Nottingham University Hospital, and three representative areas were marked on the slides. Using a Raymond Lamb tissue micro-arrayer, 1 mm cores were punched from the marked areas of the donor blocks and placed into recipient paraffin blocks to generate a tissue microarray (TMA). 4-µm sections were cut from each block for use in further experiments.

Sample preparation for MS analysis. Deparaffinization of FFPE pediatric ependymoma TMAs was achieved using an adapted protocol from Ly *et al.* (49). FFPE TMAs were first washed twice for 1 minute in a xylene bath (mixture of isomers; ≥98.5%, AnalaR NORMAPUR®, VWR, Leicestershire, UK). Residual xylene was removed and the array was allowed to dry in a fume hood for at least one hour, prior to storage at room temperature until analysis.

3D OrbiSIMS. The TMA was placed in a hybrid TOF.SIMS 5 (IONTOF GmbH, Münster, DE) instrument coupled to a Q Exactive HF (Thermo Scientific, San Jose, CA) mass spectrometer. Ions were sputtered from the surface using a 20 keV Ar_{3000+} gas cluster ion beam (GCIB). The field of view (FoV) was set to 500 µm × 500 µm. Spectra were acquired at a resolution of 20 µm in random raster mode. The Orbitrap was operated in Full-MS mode. The resolution was set to 240,000 at *m/z* 200 and the AGC target was set to 1×10^6 with a maximum ion injection of 511 ms. Data were acquired in the scan range *m/z* 75-1125 for both positive and negative polarity.

LESA-MS/MS. The TMA was placed on a universal plate holder (Advion Biosciences, Ithaca, NY) and scanned with an Epson V330 scanner. The tissue sample location was selected in LESA Points (Advion Biosciences, Ithaca, NY). Liquid extraction surface analysis-tandem mass spectrometry (LESA-MS/MS) was carried out using a TriVersa Nanomate (Advion Biosciences, Ithaca, NY) coupled to a Q Exactive plus Orbitrap mass spectrometer (Thermo Scientific, San Jose, CA). Extraction of metabolites from tissue samples was conducted with a mixture of 80% v/v methanol (CHROMASOLV®; Sigma-Aldrich,

Gillingham, UK), and 20% v/v water (CHROMASOLV®; Sigma-Aldrich, Gillingham, UK) to which MS-grade formic acid (Optima™ LC-MS grade; Fisher Scientific, Loughborough, UK) was added (end concentration 1% v/v). Brain tissue was sampled using the contact LESA approach (50) in which the solvent tip is brought into contact with the sample to minimize the solvent spread. During contact, 1.5 µL solvent (total volume: 3 µL) was dispensed on the tissue and after 15 seconds, 2.0 µL was aspirated back into the tip. The extract was introduced into the mass spectrometer via chip-based nanoelectrospray ionization (ESI Chip™, Advion Biosciences, Ithaca, NY) at 1.4 kV and 0.3 psi gas pressure (17). The mass spectrometer was operated in Full-MS/dd-MS^2 mode. MS^1 spectra were acquired in the scan range of *m/z* 70-1050. The resolution was set to 140,000 at *m/z* 200 and the AGC target was set to 3×10^6 with a maximum ion injection time of 200 ms. Data-dependent MS/MS spectra were acquired at a resolution of 17,500 at *m/z* 200. The AGC target for MS^2 scans was set to 1×10^5 with a maximum ion injection time of 50 ms. The top 20 most intense ions were isolated within a 1 *m/z* window for fragmentation. Dynamic exclusion was applied for 120 seconds per polarity. Fragmentation was carried using higher-energy collisional dissociation (HCD) using a stepped collision energy of respectively 10, 25 and 40 eV. All tissue sections were analyzed once. MS data were acquired for 2 minutes per polarity.

Ion selection for multivariate analysis. LESA-MS spectra were averaged in XCalibur (Thermo Scientific, San Jose, CA) and exported in .RAW format. 3D OrbiSIMS spectra were exported from SurfaceLab (IONTOF GmbH, Münster, DE) as .TXT files. Mass spectrometry data were further processed using MATLAB (R2017a, The MathWorks, Inc., Natick, MA; https://github.com/jorismeurs/LESAMS)**.** For LESA-MS data, files were first converted to .mzXML (32-bit) using ProteoWizard 3.0.1908 (51). Ions were selected from the spectra using the mspeaks function and ions were aligned within 5 ppm *m/z* tolerance (15, 52). Ions with >20% missing values across all samples were removed (53). Remaining missing values were imputed using *k*-nearest neighbor (*k*nn) imputation. The value of *k* was set to 10 (54).

Metabolite identification. Ion lists from MS^1 data were searched against the Human Metabolome Database (38) with 5 ppm mass tolerance for putative annotation. For MS/MS identification, LESA-MS/MS .RAW files were opened in Compound Discoverer 3.1 (Thermo Fisher). Identification was achieved using a custom workflow (**Fig. S2**). Default values were used and MS/MS spectra were compared to spectra present in mzCloud.

Statistical analysis. Ion intensity matrices were TIC normalized and log-transformed. Processed matrices were subjected to PLS-DA with leave-one-out cross-validation. The PLS-DA model was further validated using permutation testing (37). Ions with a VIP score greater than 1.5 were considered discriminative and included for univariate statistical analysis. Discriminative ions were subjected to Student's *t*-test followed by a permutation test to estimate the FDR. P-values less than 0.05 were considered significant. Significant ions were submitted for pathway analysis in MetExplore (31, 32) and further used to study intra-tumor heterogeneity in the 3D OrbiSIMS images (https://github.com/jorismeurs/SIMS_imzML). All calculations were performed in MATLAB.

Acknowledgments

This work was supported by the Engineering and Physical Sciences Research Council [grant number: EP/N006615/1]; grant name: EPSRC Programme Grant for Next Generation Biomaterials Discovery. All relevant data are available from the Nottingham Research Data Repository, under the DOI: 10.17639/nott.7062

References

1. C. D. Bennett, *et al.*, Tissue metabolite profiles for the characterisation of paediatric cerebellar tumours. *Sci. Rep.* **8**, 11992 (2018).

2. J.-P. Kilday, *et al.*, Pediatric Ependymoma: Biological Perspectives. *Mol. Cancer Res.* **7**, 765–786 (2009).

3. J. Wu, T. S. Armstrong, M. R. Gilbert, Biology and management of ependymomas. *Neuro. Oncol.* **18**, 902–913 (2016).

4. B. Messahel, *et al.*, Relapsed intracranial ependymoma in children in the UK: Patterns of relapse, survival and therapeutic outcome. *Eur. J. Cancer* **45**, 1815–1823 (2009).

5. P. Miggiels, B. Wouters, G. J. P. van Westen, A.-C. Dubbelman, T. Hankemeier, Novel technologies for metabolomics: More for less. *TrAC Trends Anal. Chem.* (2018) https:/doi.org/10.1016/J.TRAC.2018.11.021 (September 13, 2019).

6. A. Sreekumar, *et al.*, Metabolomic profiles delineate potential role for sarcosine in prostate cancer progression. *Nature* **457**, 910–914 (2009).

7. Q. Huang, *et al.*, Metabolic Characterization of Hepatocellular Carcinoma Using Nontargeted Tissue Metabolomics. *Cancer Res.* **73**, 4992–5002 (2013).

8. R. Beger, A Review of Applications of Metabolomics in Cancer. *Metabolites* **3**, 552–574 (2013).

9. R. Pandey, L. Caflisch, A. Lodi, A. J. Brenner, S. Tiziani, Metabolomic signature of brain cancer. *Mol. Carcinog.* **56**, 2355–2371 (2017).

10. C. H. Johnson, J. Ivanisevic, G. Siuzdak, Metabolomics: beyond biomarkers and towards mechanisms. *Nat. Rev. Mol. Cell Biol.* **17**, 451–459 (2016).

11. J. Kononen, *et al.*, Tissue microarrays for high-throughput molecular profiling of tumor

specimens. *Nat. Med.* **4**, 844–847 (1998).

12. M. A. Rubin, R. Dunn, M. Strawderman, K. J. Pienta, Tissue Microarray Sampling Strategy for Prostate Cancer Biomarker Analysis. *Am. J. Surg. Pathol.* **26**, 312–319 (2002).

13. H. Battifora, The Multitumor (Sausage) Tissue Block: Novel Method for Immunohistochemical Antibody Testing. *Lab. Investig.* **55**, 244–248 (1986).

14. V. Kertesz, G. J. Van Berkel, Fully automated liquid extraction-based surface sampling and ionization using a chip-based robotic nanoelectrospray platform. *J. Mass Spectrom.* **45**, 252–260 (2010).

15. Z. Hall, Y. Chu, J. L. Griffin, Liquid Extraction Surface Analysis Mass Spectrometry Method for Identifying the Presence and Severity of Nonalcoholic Fatty Liver Disease. *Anal. Chem.* **89**, 5161–5170 (2017).

16. S. R. Ellis, *et al.*, Direct Lipid Profiling of Single Cells from Inkjet Printed Microarrays. *Anal. Chem.* **84**, 9679–9683 (2012).

17. J. Meurs, *et al.*, Improved Extraction Repeatability and Spectral Reproducibility for Liquid Extraction Surface Analysis–Mass Spectrometry Using Superhydrophobic–Superhydrophilic Patterning. *Anal. Chem.* **90**, 6001–6005 (2018).

18. S. S. Basu, *et al.*, In Vitro Liquid Extraction Surface Analysis Mass Spectrometry (ivLESA-MS) for Direct Metabolic Analysis of Adherent Cells in Culture. *Anal. Chem.* **90**, 4987–4991 (2018).

19. M. K. Passarelli, *et al.*, The 3D OrbiSIMS—label-free metabolic imaging with subcellular lateral resolution and high mass-resolving power. *Nat. Methods* **14**, 1175–1183 (2017).

20. D. Beyoğlu, J. R. Idle, Metabolomics and its potential in drug development. *Biochem. Pharmacol.* **85**, 12–20 (2013).

21. S. K. Gularyan, *et al.*, Investigation of inter- and intra-tumoral heterogeneity of glioblastoma

using TOF-SIMS. *Mol. Cell. Proteomics*, mcp.RA120.001986 (2020).

22. R. M. Alberici, *et al.*, Ambient mass spectrometry: bringing MS into the “real world.” *Anal. Bioanal. Chem.* **398**, 265–294 (2010).

23. L. S. Eberlin, *et al.*, Classifying human brain tumors by lipid imaging with mass spectrometry. *Cancer Res.* **72**, 645–654 (2012).

24. L. S. Eberlin, *et al.*, Ambient mass spectrometry for the intraoperative molecular diagnosis of human brain tumors. *Proc. Natl. Acad. Sci. U. S. A.* **110**, 1611–1616 (2013).

25. M. Verma, M. J. Khoury, J. P. A. Ioannidis, Opportunities and challenges for selected emerging technologies in cancer epidemiology: Mitochondrial, epigenomic, metabolomic, and telomerase profiling. *Cancer Epidemiol. Biomarkers Prev.* **22**, 189–200 (2013).

26. S. Cuellar-Baena, *et al.*, Comparative metabolic profiling of paediatric ependymoma, medulloblastoma and pilocytic astrocytoma. *Int. J. Mol. Med.* **26**, 941–948 (2010).

27. A. H. M. Emwas, The strengths and weaknesses of NMR spectroscopy and mass spectrometry with particular focus on metabolomics research. *Methods Mol. Biol.* **1277**, 161–193 (2015).

28. S. Rabbani, A. M. Barber, J. S. Fletcher, N. P. Lockyer, J. C. Vickerman, TOF-SIMS with argon gas cluster ion beams: A comparison with C 60+. *Anal. Chem.* **83**, 3793–3800 (2011).

29. T. M. Annesley, Ion suppression in mass spectrometry. *Clin. Chem.* **49**, 1041–4 (2003).

30. K. Y. Leung, K. Mills, K. A. Burren, A. J. Copp, N. D. E. Greene, Quantitative analysis of myo-inositol in urine, blood and nutritional supplements by high-performance liquid chromatography tandem mass spectrometry. *J. Chromatogr. B Anal. Technol. Biomed. Life Sci.* **879**, 2759–2763 (2011).

31. L. Cottret, *et al.*, MetExplore: a web server to link metabolomic experiments and genome-scale metabolic networks. *Nucleic Acids Res.* **38**, W132–W137 (2010).

32. L. Cottret, *et al.*, MetExplore: collaborative edition and exploration of metabolic networks. *Nucleic Acids Res.* **46**, W495–W502 (2018).

33. S. Patel, S. Ahmed, Emerging field of metabolomics: Big promise for cancer biomarker identification and drug discovery. *J. Pharm. Biomed. Anal.* **107**, 63–74 (2015).

34. D. G. Brown, *et al.*, Metabolomics and metabolic pathway networks from human colorectal cancers, adjacent mucosa, and stool. *Cancer Metab.* **4**, 11 (2016).

35. P. Massonnet, R. M. A. Heeren, A concise tutorial review of TOF-SIMS based molecular and cellular imaging. *J. Anal. At. Spectrom.* **34**, 2217–2228 (2019).

36. B. Worley, R. Powers, Multivariate Analysis in Metabolomics. *Curr. Metabolomics* **1**, 92–107 (2013).

37. J. A. Westerhuis, *et al.*, Assessment of PLSDA cross validation. *Metabolomics* **4**, 81–89 (2008).

38. D. S. Wishart, *et al.*, HMDB 4.0: The human metabolome database for 2018. *Nucleic Acids Res.* **46**, D608–D617 (2018).

39. C. S. Yeh, *et al.*, Fatty acid metabolism pathway play an important role in carcinogenesis of human colorectal cancers by Microarray-Bioinformatics analysis. *Cancer Lett.* **233**, 297–308 (2006).

40. Q. Qu, F. Zeng, X. Liu, Q. J. Wang, F. Deng, Fatty acid oxidation and carnitine palmitoyltransferase I: Emerging therapeutic targets in cancer. *Cell Death Dis.* **7**, e2226–e2226 (2016).

41. R. C. Geck, A. Toker, Nonessential amino acid metabolism in breast cancer. *Adv. Biol. Regul.* **62**, 11–17 (2016).

42. M. J. Lukey, W. P. Katt, R. A. Cerione, Targeting amino acid metabolism for cancer therapy. *Drug Discov. Today* **22**, 796–804 (2017).

43. K. W. Pajtler, *et al.*, Molecular Classification of Ependymal Tumors across All CNS Compartments, Histopathological Grades, and Age Groups. *Cancer Cell* (2015) https:/doi.org/10.1016/j.ccell.2015.04.002.

44. B. Balluff, M. Hanselmann, R. M. A. Heeren, "Mass Spectrometry Imaging for the Investigation of Intratumor Heterogeneity" in *Advances in Cancer Research*, (Academic Press Inc., 2017), pp. 201–230.

45. C. G. Thompson, *et al.*, Mass spectrometry imaging reveals heterogeneous efavirenz distribution within putative HIV reservoirs. *Antimicrob. Agents Chemother.* **59**, 2944–2948 (2015).

46. M. A. Qazi, *et al.*, Intratumoral heterogeneity: pathways to treatment resistance and relapse in human glioblastoma. *Ann. Oncol.* **28**, 1448–1456 (2017).

47. C. A. Stewart, *et al.*, Single-cell analyses reveal increased intratumoral heterogeneity after the onset of therapy resistance in small-cell lung cancer. *Nat. Cancer* **1**, 423–436 (2020).

48. S. Ramón y Cajal, *et al.*, Clinical implications of intratumor heterogeneity: challenges and opportunities. *J. Mol. Med.* **98**, 161–177 (2020).

49. A. Ly, *et al.*, High-mass-resolution MALDI mass spectrometry imaging of metabolites from formalin-fixed paraffin-embedded tissue. *Nat. Protoc.* **11**, 1428–1443 (2016).

50. E. C. Randall, J. Bunch, H. J. Cooper, Direct analysis of intact proteins from *Escherichia coli* colonies by liquid extraction surface analysis mass spectrometry. *Anal. Chem.* **86**, 10504–10510 (2014).

51. D. Kessner, M. Chambers, R. Burke, D. Agus, P. Mallick, ProteoWizard: open source software for rapid proteomics tools development. *Bioinformatics* **24**, 2534–2536 (2008).

52. E. Gorrochategui, J. Jaumot, R. Tauler, ROIMCR: a powerful analysis strategy for LC-MS

metabolomic datasets. *BMC Bioinformatics* **20**, 256 (2019).

53. A. K. Smilde, M. J. van der Werf, S. Bijlsma, B. J. C. van der Werff-van der Vat, R. H. Jellema, Fusion of Mass Spectrometry-Based Metabolomics Data. *Anal. Chem.* **77**, 6729–6736 (2005).

54. R. Di Guida, *et al.*, Non-targeted UHPLC-MS metabolomic data processing methods: a comparative investigation of normalisation, missing value imputation, transformation and scaling. *Metabolomics* **12**, 93 (2016).